Atmos. Meas. Tech. Discuss., 7, 11137–11168, 2014
www.atmos-meas-tech-discuss.net/7/11137/2014/
doi:10.5194/amtd-7-11137-2014

Atmospheric Measurement Techniques Discussions

Scanning supersaturation CPC applied as a nano-CCN counter for size-resolved analysis of the hygroscopicity and chemical composition of nanoparticles

Z. B. Wang[1], H. Su[1], X. Wang[1], N. Ma[2], A. Wiedensohler[2], U. Pöschl[1], and Y. Cheng[1]

[1]Multiphase Chemistry Department, Max Planck Institute for Chemistry, Mainz 55020, Germany
[2]Leibniz-Institute for Tropospheric Research, Leipzig 04318, Germany

Received: 18 October 2014 – Accepted: 24 October 2014 – Published: 17 November 2014

Correspondence to: H. Su (h.su@mpic.de) and Y. Cheng (yafang.cheng@mpic.de)

Published by Copernicus Publications on behalf of the European Geosciences Union.

Abstract

Chemical composition is essential for understanding the formation and evolution of atmospheric aerosol particles. Due to analytical limitations, however, relatively little information is available for sub-10 nm particles. We present the design of a nano-cloud condensation nuclei counter (nano-CCNC) for measuring size-resolved hygroscopicity and inferring chemical composition of sub-10 nm aerosol particles. We extend the use of counting efficiency spectra from a water-based condensation particle counter (CPC) and link it to the analysis of CCN activation spectra, which provides a theoretical basis for the application of a scanning supersaturation CPC (SS-CPC) as a nano-CCNC. Measurement procedures and data analysis methods are demonstrated through laboratory experiments with monodisperse particles of diameter down to 2.5 nm, where sodium chloride, ammonium sulfate, sucrose and tungsten oxide can be easily discriminated by different characteristic supersaturations of water droplet formation. The design is not limited to the water CPC, but also applies to CPCs with other working fluids (e.g. butanol, perfluorotributylamine). We suggest that a combination of SS-CPCs with multiple working fluids may provide further insight into the chemical composition of nanoparticles and the role of organic and inorganic compounds in the initial steps of atmospheric new particle formation and growth.

1 Introduction

New particle formation (NPF) and subsequent growth have been intensively studied owning to their important roles in air pollution and climate (Kulmala et al., 2000, 2013, 2014; Kerminen et al., 2012; Zhang et al., 2012). Chemical composition of the newly formed particles is key to understand the production and transformation of atmospheric aerosol particles. A number of apparatuses have been developed to analyze the chemical compositions of ultrafine particles (Fig. 1). Despite these progresses, there is still

AMTD
7, 11137–11168, 2014

a gap in the size range of 1–10 nm where chemical composition can be hardly measured.

The ability of aerosol particles to serve as cloud condensation nuclei (CCN), i.e., to initiate the formation of droplets by condensation of water vapor, is closely linked to their chemical composition. Size-resolved measurements have shown that atmospheric aerosol particle hygroscopicity and CCN activity are closely correlated with particle composition expressed as organic and inorganic mass fractions determined by aerosol mass spectrometry (Dusek et al., 2006, 2010; Gunthe et al., 2009, 2011; Jurányi et al., 2010; Rose et al., 2010, 2011, 2013; Cerully et al., 2011; Lance et al., 2013; Lathem et al., 2013; Mei et al., 2013; Wu et al., 2013). Hygroscopicity distributions derived from size-resolved CCN measurements also provide insight into the mixing state of aerosol particles (Lance, 2007; Su et al., 2010). Widely used CCN counters based on the continuous-flow thermal gradient technique can potentially measure at water vapor supersaturations up to 6 % (S = (saturation ratio – 1) × 100 %; Lance et al., 2006). Traditionally, however, atmospheric CCN measurements were mostly focusing on supersaturations less than ∼ 1 % corresponding to particle sizes above ∼ 30 nm as referenced above. For the activation of sub-10 nm particles, higher levels of water vapor supersaturation are required as shown in Fig. 2 as a function of particle size and hygroscopicity. In the atmosphere, supersaturations > 1 % are less common but do occur in convective clouds (Pruppacher and Klett, 1997), especially at low aerosol concentrations and high updraft velocities (aerosol-limited regime of CCN activation; Pöschl et al., 2010).

In this study, we present the concept of a nano-CCNC for measuring hygroscopicity and inferring chemical composition of nanoparticles in the diameter range of ∼ 2–10 nm. The method builds on recent progresses in size-resolved CCN measurements of ultrafine aerosol particles as referenced above. We first explain the theoretical basis, instrument setup and the data retrieval methodology. Subsequently, we report experimental data for a proto-type nano-CCNC and its performance in discriminating

AMTD
7, 11137–11168, 2014

different substances. Finally, we discuss potential applications of the nano-CCNC in field and laboratory experiments in combination with other techniques.

2 Design and operation

2.1 CPC vs. CCNC

The activation of sub-10 nm particles with water vapor requires a higher supersaturation S, which goes beyond the measurement range of most CCN counters, but falls into the range of water-based condensation particle counters (CPC). The water CPC is based on a similar working principle as a CCNC but running at a much higher S. High S reduces the critical activation size of particles so that "almost all" interested particles can be activated and detected (McMurry, 2000b, a). In theory, the counting efficiency curve of CPC is the same as the activation curve of CCNC, but extended to smaller size ranges (Fig. 3).

In practice, CPCs and CCNCs have different applications by making use of different parts of their activation curves. As shown in Fig. 3, the CPC is mainly used for the accurate particle counting, ideally operated at size ranges with activation fractions (F_{act}) equal to 1. The size-resolved CCN measurements are often designed to determine the whole activation curves, especially the composition-sensitive parts with F_{act} varying between 0 and 1.

2.2 Design and operation of nano-CCNC

Our nano-CCNC system adopted a similar design from previous size-resolved CCN measurements (Rose et al., 2008; Moore et al., 2010). It comprises of a nano-differential mobility analyzer (nano-DMA, TSI model 3085), a total particle counter (electrometer or ultrafine CPC with smaller critical detection size) and a nano-CCNC along with drying system and a neutralizer (TSI model 3077). The nano-CCNC is a water-based CPC with a control unit regulating the scan of S.

AMTD
7, 11137–11168, 2014

The measuring protocol of nano-CCNC is (1) to use a nano-DMA to select monodisperse particles of certain dry diameter (D_d); and (2) to measure the number concentration of total particles (N_{tot}) by the total particle counter and activated particles (N_{act}) at varied S by SS-CPC, respectively. This results in a size and superaturation-resolved activation fraction, $F_{act} = f(D_d, S)$. By scanning D_d and S, the whole 3-D activation spectra over the $D_d - S$ plane can be achieved (Su et al., 2010). In practice, people can first keep D_d constant and vary S, then select another value of D_d and iterate the procedure as the "S scan" mode in CCN measurements (Dusek et al., 2006; Moore and Nenes, 2009; Snider et al., 2010). Alternatively, we could also first keep S constant and vary D_d as the "D_d scan" mode (Petters et al., 2009; Wiedensohler et al., 2009; Rose et al., 2011).

The scan of S can be achieved by scanning the temperature gradient between the saturator and growth tube (by changing the saturator or growth tube temperature; Mordas et al., 2008; Kupc et al., 2013) or scanning the aerosol flow rate of the CPC (Gallar et al., 2006; Wimmer et al., 2013). The former approach, however, has not been actively pursued partly due to the relatively slow thermal response, limiting the time resolution of measurement to tens of minutes with current CPCs (McDermott et al., 1991). However, if we are only interested in a narrow size ranges, i.e., sub-10 nm or even a single size, it is still a feasible option, because relatively small number of sizes needs to be scanned. The scanning flow approach has better time resolution. In the work of Gallar et al. (2006), the flow scan is achieved by varying the mixing ratio of saturator and dilution air and their main purpose is to obtain particle size spectrum. After using fast-response flow controllers, time response of CPC (with a perfluorinated organic compound as the working fluid) could reach ~ 1 s to the change of supersaturation.

2.3 Measurement procedure and data analysis

Concerning the application of nano-CCNC, we proposed the following procedure as shown in Fig. 4b. The first step is to characterize the calibration curve, i.e., the cumulative supersaturation distribution that aerosol particles experienced in the CPCs, which

AMTD
7, 11137–11168, 2014

will then be used to determine the characteristic activation supersaturation of aerosol samples for inferring chemical composition.

2.3.1 Determination of supersaturation distribution

For particles of the same composition, their ideal activation curves would be a step function according to the Köhler theory. However, the observed activation curves in Fig. 3 turn out to be a rather broad distribution. The broadening of the activation curves can be attributed to (1) the non-uniform S that particles have been exposed to in the CPC, (2) the transfer function of DMA, especially for smaller nanoparticles due to diffusional effects (Stolzenburg, 1988), and (3) the doubly/multiply charged particles. The influence of doubly/multiply charged particles can be minimized by carefully adjusting the size distribution of calibration aerosols (so that the investigated diameter lies on the right side of the mode diameter of calibration aerosols). The diffusion of nanoparticles in the CPC causes the non-uniformity of exposed S, which results in a broadening effect much larger than that from the DMA transfer function. For example, at particle diameter of ~ 2–3 nm, the DMA transfer function (TSI nano-DMA model 3085) only contributes to ~ 36 % of the overall broadened width while the rest can be attributed to the non-uniformity of S. The value of 36 % is calculated from a ~ 18 % NFWHM (normalized full-width at half-maximum) of the DMA transfer function (Chen et al., 1998; Stolzenburg and McMurry, 2008; Jiang et al., 2011b) and a ~ 50 % NFWHM for the observed activation curves (Kupc et al., 2013).

Figure 5 explains the origin of non-uniformity of exposed S in the CPC. In the aerosol activation unit (growth tube, Fig. 5a), S is not evenly distributed and the maximum S appears in the centerline (Fig. 5b). Though a sheath flow is used to focus the aerosol samples, the paths of nanoparticles could still deviate from the centerline due to dispersions (Stolzenburg and McMurry, 1991). Thus particles of the same properties can either be activated or not depending on its exposed S (only the portion of particles that experienced S higher than its critical supersaturation (S_{cri}) can be activated, Fig. 5d). That is why a broadened activation curve was observed instead of a step function as

AMTD
7, 11137–11168, 2014

shown in Fig. 3. The S distribution that particles experience depends on the spatial distribution of S in the CPC and the path taken by the particles.

By assuming a dominant role of S non-uniformity in the broadening effect, we have the following a mathematical expression for the observed activated fraction $F_{act}(D_d)$:

$$F_{act}(D_d) = \frac{\int n_N(S)(1 - H(S))dS}{\int n_N(S)dS} = \frac{\int n_N(S)(1 - H(S))dS}{N_{tot}}$$
$$= \int \frac{n_N(S)}{N_{tot}}(1 - H(S))dS = \int n_N^*(S)(1 - H(S))dS \quad (1)$$

where $H(S)$ can be regarded as the a cumulative distribution function (CDF) of effective S inside the CPC (i.e., the fraction of particles experiencing a supersaturation lower than or equal to the value of S); $n_N(S)$ is the aerosol number distribution as functions of its critical activation supersaturation; $n_N(S)dS$ equals number concentration of particles in the critical supersaturation range of S to $S + dS$ and $n_N^*(S) = n_N(S)/N_{tot}$ is the normalized distribution. According to the Köhler theory, particles of identical size and composition have the same critical supersaturation S_{cri} and the corresponding $n_N^*(S)$ becomes a Dirac delta function, or δ function. Substituting $n_N^*(S) = \delta(S - S_{cri})$ into Eq. (1) gives

$$F_{act}(D_d) = \int \delta(S - S_{cri})(1 - H(S_{cri}))dS = 1 - H(S_{cri}) \quad (2)$$

Then we have the value of the cumulative distribution function at S_{cri}, $H(S_{cri}) = 1 - F_{act}(D_d)$. By changing S_{cri} of aerosol samples, we could scan through the S space and get the whole distribution of $H(S)$. In practice, the scanning of supersaturation can be achieved by scanning D_d. Equation (2) is actually suggesting that the supersaturation distribution $H(S)$ that aerosol particles experience in the CPC can be determined from counting efficiency spectra of compounds whose activation function is known (so that S_{cri} can be directly calculated from D_d based on the Köhler equation).

AMTD
7, 11137–11168, 2014

2.3.2 Determination of characteristic supersaturations

Once the whole distribution $H(S) = f(S)$ is determined, the characteristic activation S for a monodisperse unknown compounds can be directly calculated from its inverse function:

$$S = f^{-1}(H) = f^{-1}(1 - F_{act}) \quad (3)$$

Equation (3) refers to monodisperse particles of a single activation S. It becomes more complicated when monodisperse particles with multiple activation supersaturations are considered (externally mixed aerosol particles). The mathematical solution to this problem is explained as follows. By discretizing the right hand side of Eq. (1) into J bins, we have F_{act} as a linear combination of n^*_N

$$F_{act,i} = \sum^{J} n^*_N(S_j)(1 - H_i(S_j))\Delta S = \sum^{J} a_{i,j}x_j \quad (4)$$

where j denotes the bin number of S; i denotes the ith $H(S)$ distribution (because we can measure the same kind of aerosol particles with CPCs of different H). The $a_{i,j}$ and x_j are introduced here for simple illustration, in which $a_{i,j}$ is a known parameter, $a_{i,j} = (1 - H_i(S_j))\Delta S$ and $x_j = n^*_N$ is an unknown. Finally, $n_N{}^*$ can be solved by constructing a series of independent equations, i.e. total number of i, I, should meet the equation with: $I \geq J$. A complete data retrieval method will be presented in a following paper, in which the DMA transfer function, size dependence of $H(S)$, particle shape factors and mixing states will be considered along with the S distribution.

2.3.3 Ambient measurement

With a given activation fraction F_{act}, we can infer the S_{cri} from the supersaturation distribution $H(S)$. However, in most cases, the low concentration/count of sub-10 nm particles challenges our instrument because the electrometer can only be operated reliably

AMTD
7, 11137–11168, 2014

at high concentration level (> 1000 cm^{-3}; Wiedensohler et al., 1994), which is basically never the case for size-resolved measurement at ambient condition. To overcome this problem, we propose the use of relative activation ratio R_{H/H_0}, which is defined as the ratio of activation fraction at one $H(S)$ distribution to that of the other $H_0(S)$ distribution:

$$R_{H/H_0} = F_{act,T}/F_{act,T_0} = (N_{act,T}/N_{tot})/(N_{act,T_0}/N_{tot}) = N_{act,T}/N_{act,T_0} \quad (5)$$

in which T and T_0 correspond to the different saturator temperature T_s, $N_{act,T}$ and N_{act,T_0} are CPC counts at T and T_0, respectively. On the other hand, R_{H/H_0} can be determined from two $H(S)$ characterized by calibration aerosols:

$$R_{H/H_0} = \frac{1 - H_T(S)}{1 - H_{T_0}(S)} = g(S) \quad (6)$$

Then the same as Eq. (2), once R_{H/H_0} is measured, we can determine:

$$S_{cri} = g^{-1}(R_{H/H_0}) = g^{-1}(N_{act,T}/N_{act,T_0}) \quad (7)$$

According to Eq. (5), R_{H/H_0} can be measured by two CPCs with different saturator temperature. Electrometer is not needed in this case and the corresponding detection limit problem no longer exists.

3 Results and discussion

In the following sections, we will demonstrate the proposed methods with laboratory experimental data for different aerosol particles. We first used tungsten oxide (WO_x) particles for the determination of $H(S)$, and then calculated the characteristic S_{cri} for different kinds of 2.5 nm particles.

AMTD
7, 11137–11168, 2014

3.1 Supersaturation distribution

In this study, WO_x particles, produced by a WO_x generator (Grimm Aerosol Technik, Nano WO_x-generator, model 7.860; Wimmer et al., 2013), was used to determine the $H(S)$ under different saturator temperatures. As demonstrated in Fig. 4a, a water-based CPC (TSI model 3788) was used as a SS-CPC to measure N_{act} and a Faraday Cup Electrometer (Grimm Aerosol Technik, model 5.705) was used to measure N_{tot}. The S distribution that particles experienced inside the water-based CPC, $H(S)$, was achieved by measuring the counting efficiency spectra from 2 to 10 nm. Seven $H(S)$ distributions were measured with saturator temperature (T_s) varying from 284 to 296 K, while the growth tube temperature (T_{gt}) was fixed at 348 K. Each temperature adjustment takes 150 s for stabilization.

Following Eq. (2), we retrieve $H(S)$ from the counting efficiency spectra for WO_x particles (Fig. 6). As expected, $H(S)$ was changed considerably by tuning the saturator temperature. Increasing the saturator temperature will reduce the temperature gradient and the supersaturation inside the growth tube. During the data retrieval process, we found that the activation curves for WO_x particles represent a bimodal distribution. The following expression of a bimodal lognomal CDF was used to fit the activation curves:

$$F_{act} = (50 - a) \times \left(1 + \mathrm{erf}\left(\frac{D_d - D_1}{\sigma_1\sqrt{2}}\right)\right) + a \times \left(1 + \mathrm{erf}\left(\frac{D_d - D_2}{\sigma_2\sqrt{2}}\right)\right) \quad (8)$$

Here, "erf" is the Gauss error function, a is the number fraction for one mode, D_1 and D_2 are the geometric mean values of particle diameter, and σ_1 and σ_2 are the standard deviations of the cumulative Gaussian distribution function.

For the conversion of D_d to S_{cri}, we adopt the multilayer adsorption theory accounting for the very low solubility and hygroscopicity for WO_x particles. The basic idea is to include an adsorption isotherm (FHH (Frenkel, Halsey and Hill) isotherm in this study)

AMTD
7, 11137–11168, 2014

in the traditional Köhler theory instead of the solute term:

$$S = \exp\left(\frac{4\sigma M_w}{RT\rho_w D}\right)\exp\left(-A\Theta^{-B}\right) \quad (9)$$

where σ is the surface tension; D is the diameter of solution droplet; M_w and ρ_w are the molar mass and density of water; R is the universal gas constant and T is absolute temperature. The parameter A characterizes interactions between adsorbed molecules and between the surface and adjacent adsorbate molecules and B characterizes the attraction between the solid surface and the adsorbate in subsequent layers. For further details concerning the derivation and explanation of Eq. (9), we refer the reader to Sorjamaa and Laaksonen (2007).

The evaluation of parameters A and B in Eq. (9) are determined by the best fitting between measured and calculated activated fractions F_{act} for ammonium sulfate (AS) particles at 2.5 nm (Fig. 7), with values of 0.1 and 2.1, respectively. These values are located in the range of previous literature reports ($0.1 < A < 3$, $0.5 < B < 3$; Sorjamaa and Laaksonen, 2007, and references therein). Our calculations suggest that with the appropriate parameter values, the activated fractions can be well predicted by the modified Köhler equation with FHH isotherm for the insoluble particles. For sodium chloride (NaCl) particles, it is difficult to predict F_{act} due to its uncertain shape factor. However, if we assume the volume equivalent diameter of ~ 2.1 nm, we will get similar results as shown in Fig. 7.

3.2 Characteristic S for 2.5 nm particles

For the determination of S_{cri}, we choose 2.5 nm as the target diameter and select monodisperse NaCl, AS and sucrose particles as examples. An electrospray aerosol generator (TSI model 3480) was used to produce their nanoparticles. All solutions were prepared in a standard 20 mM ammonium acetate buffer solution with a conductivity of 0.2 S m^{-1} (siemens per meter; Chen et al., 1995; Kupc et al., 2013). The activation

AMTD
7, 11137–11168, 2014

fractions were determined from results of the electrometer and SS-CPC. Seven saturator temperatures from 284 to 296 K were tested in our experiments.

Figure 8a shows distinct activation curves of various chemical compounds at 2.5 nm. For the same T_s (or $H(S)$), NaCl shows the highest activation fraction F_{act} while WO_x shows the lowest, which is consistent with their hygroscopicities. To reach the same F_{act} as NaCl, AS would require a ~ 4 K lower T_s, i.e., a larger temperature gradient and S while a further lower T_s (~ 10 K) is needed for sucrose. Such difference in the temperature gradient is significant enough in discriminating the investigated nanoparticles, much higher than the instrument noise ~ 0.1 K. The Hygroscopic Tandem Differential Mobility Analyzer (HTDMA) has been applied with D_d down to ~ 6 nm (Biskos et al., 2006a, b; Swietlicki et al., 2008), while size-resolved measurements by traditional CCN counters are limited to $D_d > 30$ nm as aforementioned. We now push this limit down to 2.5 nm.

Figure 8b shows the calculated S_{cri} for various chemical compounds at 2.5 nm. Good agreement between the estimated and theoretical supersaturation has been achieved for AS particles, as indicated in Fig. 7. In summary, our results demonstrate that based on the determined $H(S)$ distributions, the chemical compounds with different hygroscopicity can be separated distinctly, especially between representative inorganic (AS, $S = 55\% \pm 5\%$) and organic (sucrose, $S = 67\% \pm 1\%$) compounds.

As aforementioned, the detection sensitivity of the electrometer precludes its application in ambient measurement. We suggest using the relative activation ratio R_{H/H_0} as an alternative parameter. As shown in Fig. 9, different compounds (NaCl, AS, sucrose and WO_x) exhibit distinct R_{H/H_0} distributions (the ratio of $F_{act,T}$ to $F_{act,11\,°C}$). Their characteristic S_{cri} can also be determined from R_{H/H_0} by Eq. (5). It has been suggested that the major compositions of newly formed particles are sulfate and organics (Zhang et al., 2012; Almeida et al., 2013; Ehn et al., 2014), which corresponds to the envelope between the AS and WO_x profiles in Fig. 9.

AMTD
7, 11137–11168, 2014

3.3 Solvoscopicity and SS-CPCB

The concept of scanning supersaturation (SS) is not limited to water-based CPCs, and may also work for CPCs with other working fluids. In analogy to aerosol "hygroscopcity" describing the affinity for water, we introduce the term "solvoscopicty", which from a broad sense, is the ability of a substance to attract and hold solvent molecules. Substances showing higher solvoscopicity for one working liquid may have lower solvoscopicity for another working liquid (Kangasluoma et al., 2014). For example, Fig. 10a and b show that NaCl is more hygroscopic (higher S_{cri} and lower D_{cri}) than Ag but become less "solvoscopic" in butanol vapor.

The solvoscopic parameter can be used as "footprint" to estimate/distinguish the aerosol composition. However, it does not work once different substances show similar solvoscopicities, e.g., as sucrose and emery oil in butanol (Fig. 10c). This problem can be solved by performing additional measurements with water-based CPC, in which sucrose and emery oil show distinct hygroscopicities. Therefore, we suggest running multiple CPCs with different working fluids in a SS mode, which gives a SS-CPCB (SS-CPC battery) system. Compared to a single SS-CPC, SS-CPCB results in a multiple dimension of S_{cri} enabling better inference of chemical composition. As shown in Fig. 10c, different inorganic and organic substances as well as metal can be easily distinguished in the 2-D solvoscopiciy matrix. Compared to earlier applications of (nano-)CPCB (Kulmala et al., 2007; Riipinen et al., 2009; Kangasluoma et al., 2014), the SS-CPCB system could provide size-resolved solvoscopicity information for each working fluid, while CPCB present integrated information over certain size ranges.

4 Conclusion and outlook

In this study, we present the theoretical basis and design of a nano-CCN counter for the purpose of hygroscopicity measurement in the nano size range (sub-10 nm). The basic concept is to operate a water-based CPC in a scanning supersaturation mode

AMTD
7, 11137–11168, 2014

as a CCNC, recording a composition-dependent activated spectrum and retrieving the solvoscopicity parameter/distribution.

The proof-of-principle experiments were carried out with 2.5 nm sodium chloride, ammonium sulfate, sucrose and tungsten oxide particles, which show a clear composition dependency and reproducibility of the activation spectra. By using calibration aerosols (WO_x), we show the importance of using activation fraction $F_{act}(D_d)$ of aerosol samples to calibrate $H(S)$ inside CPC at different saturator temperatures and its use in further retrieval of aerosol hygroscopicities.

Though termed as nano-CCNC, the design is not limited to the water-based CPC, but also applies to CPCs with other working fluids. We introduce the term "solvoscopicty" to describe the ability of a substance to attract and hold solvent molecules. Substance solvoscopicity might vary in different working fluids. Compared with single SS-CPC, the SS-CPCB, a combination of CPCs with multiple working fluids in a SS mode, might hence provide further insight into the chemical composition of nanoparticles.

In addition, pulse-height spectral analysis has been used to investigate the chemical composition of newly formed particles (Marti et al., 1996; Saros et al., 1996; Weber et al., 1998; O'Dowd et al., 2004; Gallar et al., 2006). The combination of activation fraction and pulse-height spectra will be explored in our future study.

Acknowledgements. This study was supported by the Max Planck Society (MPG), the European Commission under the projects PEGASOS (grant No. 265148), BACCHUS (grant No. 603445), and National Science Foundation of China (NSFC, grant No. 41330635). We gratefully acknowledge P. H. McMurry, T. Klimach, J. Schneider, T. Tritscher (from TSI GmbH), F. Tettich and C. Kunath (from GRIMM Aerosol Technik) for encouraging discussions, instrumentation and technical support.

The service charges for this open access publication have been covered by the Max Planck Society.

AMTD
7, 11137–11168, 2014

References

Almeida, J., Schobesberger, S., Kurten, A., Ortega, I. K., Kupiainen-Maatta, O., Praplan, A. P., Adamov, A., Amorim, A., Bianchi, F., Breitenlechner, M., David, A., Dommen, J., Donahue, N. M., Downard, A., Dunne, E., Duplissy, J., Ehrhart, S., Flagan, R. C., Franchin, A., Guida, R., Hakala, J., Hansel, A., Heinritzi, M., Henschel, H., Jokinen, T., Junninen, H., Kajos, M., Kangasluoma, J., Keskinen, H., Kupc, A., Kurten, T., Kvashin, A. N., Laaksonen, A., Lehtipalo, K., Leiminger, M., Leppa, J., Loukonen, V., Makhmutov, V., Mathot, S., McGrath, M. J., Nieminen, T., Olenius, T., Onnela, A., Petaja, T., Riccobono, F., Riipinen, I., Rissanen, M., Rondo, L., Ruuskanen, T., Santos, F. D., Sarnela, N., Schallhart, S., Schnitzhofer, R., Seinfeld, J. H., Simon, M., Sipila, M., Stozhkov, Y., Stratmann, F., Tome, A., Trostl, J., Tsagkogeorgas, G., Vaattovaara, P., Viisanen, Y., Virtanen, A., Vrtala, A., Wagner, P. E., Weingartner, E., Wex, H., Williamson, C., Wimmer, D., Ye, P., Yli-Juuti, T., Carslaw, K. S., Kulmala, M., Curtius, J., Baltensperger, U., Worsnop, D. R., Vehkamaki, H., and Kirkby, J.: Molecular understanding of sulphuric acid-amine particle nucleation in the atmosphere, Nature, 502, 359–363, doi:10.1038/nature12663, 2013.

Biskos, G., Malinowski, A., Russell, L. M., Buseck, P. R., and Martin, S. T.: Nanosize effect on the deliquescence and the efflorescence of sodium chloride particles, Aerosol Sci. Tech., 40, 97–106, doi:10.1080/02786820500484396, 2006a.

Biskos, G., Russell, L. M., Buseck, P. R., and Martin, S. T.: Nanosize effect on the hygroscopic growth factor of aerosol particles, Geophys. Res. Lett., 33, L07801, doi:10.1029/2005GL025199, 2006b.

Cerully, K. M., Raatikainen, T., Lance, S., Tkacik, D., Tiitta, P., Petäjä, T., Ehn, M., Kulmala, M., Worsnop, D. R., Laaksonen, A., Smith, J. N., and Nenes, A.: Aerosol hygroscopicity and CCN activation kinetics in a boreal forest environment during the 2007 EUCAARI campaign, Atmos. Chem. Phys., 11, 12369–12386, doi:10.5194/acp-11-12369-2011, 2011.

Chen, D.-R., Pui, D. Y. H., and Kaufman, S. L.: Electrospraying of conducting liquids for monodisperse aerosol generation in the 4 nm to 1.8 µm diameter range, J. Aerosol Sci., 26, 963–977, doi:10.1016/0021-8502(95)00027-A, 1995.

Chen, D. R., Pui, D. Y. H., Hummes, D., Fissan, H., Quant, F. R., and Sem, G. J.: Design and evaluation of a nanometer aerosol differential mobility analyzer (Nano-DMA), J. Aerosol Sci., 29, 497–509, doi:10.1016/S0021-8502(97)10018-0, 1998.

AMTD
7, 11137–11168, 2014

Dusek, U., Frank, G. P., Hildebrandt, L., Curtius, J., Schneider, J., Walter, S., Chand, D., Drewnick, F., Hings, S., Jung, D., Borrmann, S., and Andreae, M. O.: Size matters more than chemistry for cloud-nucleating ability of aerosol particles, Science, 312, 1375–1378, doi:10.1126/science.1125261, 2006.

Dusek, U., Frank, G. P., Curtius, J., Drewnick, F., Schneider, J., Kürten, A., Rose, D., Andreae, M. O., Borrmann, S., and Pöschl, U.: Enhanced organic mass fraction and decreased hygroscopicity of cloud condensation nuclei (CCN) during new particle formation events, Geophys. Res. Lett., 37, L03804, doi:10.1029/2009GL040930, 2010.

Ehn, M., Thornton, J. A., Kleist, E., Sipila, M., Junninen, H., Pullinen, I., Springer, M., Rubach, F., Tillmann, R., Lee, B., Lopez-Hilfiker, F., Andres, S., Acir, I.-H., Rissanen, M., Jokinen, T., Schobesberger, S., Kangasluoma, J., Kontkanen, J., Nieminen, T., Kurten, T., Nielsen, L. B., Jorgensen, S., Kjaergaard, H. G., Canagaratna, M., Maso, M. D., Berndt, T., Petaja, T., Wahner, A., Kerminen, V.-M., Kulmala, M., Worsnop, D. R., Wildt, J., and Mentel, T. F.: A large source of low-volatility secondary organic aerosol, Nature, 506, 476–479, doi:10.1038/nature13032, 2014.

Gallar, C., Brock, C. A., Jimenez, J. L., and Simons, C.: A variable supersaturation condensation particle sizer, Aerosol Sci. Tech., 40, 431–436, doi:10.1080/02786820600643339, 2006.

Gunthe, S. S., King, S. M., Rose, D., Chen, Q., Roldin, P., Farmer, D. K., Jimenez, J. L., Artaxo, P., Andreae, M. O., Martin, S. T., and Pöschl, U.: Cloud condensation nuclei in pristine tropical rainforest air of Amazonia: size-resolved measurements and modeling of atmospheric aerosol composition and CCN activity, Atmos. Chem. Phys., 9, 7551–7575, doi:10.5194/acp-9-7551-2009, 2009.

Gunthe, S. S., Rose, D., Su, H., Garland, R. M., Achtert, P., Nowak, A., Wiedensohler, A., Kuwata, M., Takegawa, N., Kondo, Y., Hu, M., Shao, M., Zhu, T., Andreae, M. O., and Pöschl, U.: Cloud condensation nuclei (CCN) from fresh and aged air pollution in the megacity region of Beijing, Atmos. Chem. Phys., 11, 11023–11039, doi:10.5194/acp-11-11023-2011, 2011.

Hermann, M., Wehner, B., Bischof, O., Han, H. S., Krinke, T., Liu, W., Zerrath, A., and Wiedensohler, A.: Particle counting efficiencies of new TSI condensation particle counters, J. Aerosol Sci., 38, 674–682, doi:10.1016/j.jaerosci.2007.05.001, 2007.

Iida, K., Stolzenburg, M. R., and McMurry, P. H.: Effect of working fluid on sub-2 nm particle detection with a laminar flow ultrafine condensation particle counter, Aerosol Sci. Tech., 43, 81–96, doi:10.1080/02786820802488194, 2009.

AMTD
7, 11137–11168, 2014

Jayne, J. T., Leard, D. C., Zhang, X., Davidovits, P., Smith, K. A., Kolb, C. E., and Worsnop, D. R.: Development of an aerosol mass spectrometer for size and composition analysis of submicron particles, Aerosol Sci. Tech., 33, 49–70, doi:10.1080/027868200410840, 2000.

Jiang, J., Zhao, J., Chen, M., Eisele, F. L., Scheckman, J., Williams, B. J., Kuang, C., and McMurry, P. H.: First measurements of neutral atmospheric cluster and 1–2 nm particle number size distributions during nucleation events, Aerosol Sci. Tech., 45, ii–v, doi:10.1080/02786826.2010.546817, 2011a.

Jiang, J. K., Attoui, M., Heim, M., Brunelli, N. A., McMurry, P. H., Kasper, G., Flagan, R. C., Giapis, K., and Mouret, G.: Transfer functions and penetrations of five differential mobility analyzers for sub-2 nm particle classification, Aerosol Sci. Tech., 45, 480–492, 2011b.

Jokinen, T., Sipilä, M., Junninen, H., Ehn, M., Lönn, G., Hakala, J., Petäjä, T., Mauldin III, R. L., Kulmala, M., and Worsnop, D. R.: Atmospheric sulphuric acid and neutral cluster measurements using CI-APi-TOF, Atmos. Chem. Phys., 12, 4117–4125, doi:10.5194/acp-12-4117-2012, 2012.

Jurányi, Z., Gysel, M., Weingartner, E., DeCarlo, P. F., Kammermann, L., and Baltensperger, U.: Measured and modelled cloud condensation nuclei number concentration at the high alpine site Jungfraujoch, Atmos. Chem. Phys., 10, 7891–7906, doi:10.5194/acp-10-7891-2010, 2010.

Kangasluoma, J., Kuang, C., Wimmer, D., Rissanen, M. P., Lehtipalo, K., Ehn, M., Worsnop, D. R., Wang, J., Kulmala, M., and Petäjä, T.: Sub-3 nm particle size and composition dependent response of a nano-CPC battery, Atmos. Meas. Tech., 7, 689–700, doi:10.5194/amt-7-689-2014, 2014.

Kerminen, V.-M., Paramonov, M., Anttila, T., Riipinen, I., Fountoukis, C., Korhonen, H., Asmi, E., Laakso, L., Lihavainen, H., Swietlicki, E., Svenningsson, B., Asmi, A., Pandis, S. N., Kulmala, M., and Petäjä, T.: Cloud condensation nuclei production associated with atmospheric nucleation: a synthesis based on existing literature and new results, Atmos. Chem. Phys., 12, 12037–12059, doi:10.5194/acp-12-12037-2012, 2012.

Kulmala, M., Pirjola, L., and Makela, J. M.: Stable sulphate clusters as a source of new atmospheric particles, Nature, 404, 66–69, 2000.

Kulmala, M., Mordas, G., Petäjä, T., Grönholm, T., Aalto, P. P., Vehkamäki, H., Hienola, A. I., Herrmann, E., Sipilä, M., Riipinen, I., Manninen, H. E., Hämeri, K., Stratmann, F., Bilde, M., Winkler, P. M., Birmili, W., and Wagner, P. E.: The condensation particle counter battery

AMTD
7, 11137–11168, 2014

(CPCB): a new tool to investigate the activation properties of nanoparticles, J. Aerosol Sci., 38, 289–304, doi:10.1016/j.jaerosci.2006.11.008, 2007.

Kulmala, M., Kontkanen, J., Junninen, H., Lehtipalo, K., Manninen, H. E., Nieminen, T., Petäjä, T., Sipilä, M., Schobesberger, S., Rantala, P., Franchin, A., Jokinen, T., Järvinen, E., Äijälä, M., Kangasluoma, J., Hakala, J., Aalto, P. P., Paasonen, P., Mikkilä, J., Vanhanen, J., Aalto, J., Hakola, H., Makkonen, U., Ruuskanen, T., Mauldin, R. L., Duplissy, J., Vehkamäki, H., Bäck, J., Kortelainen, A., Riipinen, I., Kurtén, T., Johnston, M. V., Smith, J. N., Ehn, M., Mentel, T. F., Lehtinen, K. E. J., Laaksonen, A., Kerminen, V.-M., and Worsnop, D. R.: Direct observations of atmospheric aerosol nucleation, Science, 339, 943–946, doi:10.1126/science.1227385, 2013.

Kulmala, M., Petäjä, T., Ehn, M., Thornton, J., Sipilä, M., Worsnop, D. R., and Kerminen, V.-M.: Chemistry of atmospheric nucleation: on the recent advances on precursor characterization and atmospheric cluster composition in connection with atmospheric new particle formation, Annu. Rev. Phys. Chem., 65, 21–37, doi:10.1146/annurev-physchem-040412-110014, 2014.

Kupc, A., Bischof, O., Tritscher, T., Beeston, M., Krinke, T., and Wagner, P. E.: Laboratory characterization of a new nano-water-based CPC 3788 and performance comparison to an ultrafine butanol-based CPC 3776, Aerosol Sci. Tech., 47, 183–191, doi:10.1080/02786826.2012.738317, 2013.

Lance, S.: Quantifying compositional impacts of ambient aerosol on cloud droplet formation, Ph. D. thesis, Georgia Institute of Technology, Atlanta, GA, 2007.

Lance, S., Nenes, A., Medina, J., and Smith, J. N.: Mapping the operation of the DMT Continuous Flow CCN Counter, Aerosol Sci. Tech., 40, 242–254, doi:10.1080/02786820500543290, 2006.

Lance, S., Raatikainen, T., Onasch, T. B., Worsnop, D. R., Yu, X.-Y., Alexander, M. L., Stolzenburg, M. R., McMurry, P. H., Smith, J. N., and Nenes, A.: Aerosol mixing state, hygroscopic growth and cloud activation efficiency during MIRAGE 2006, Atmos. Chem. Phys., 13, 5049–5062, doi:10.5194/acp-13-5049-2013, 2013.

Lathem, T. L., Beyersdorf, A. J., Thornhill, K. L., Winstead, E. L., Cubison, M. J., Hecobian, A., Jimenez, J. L., Weber, R. J., Anderson, B. E., and Nenes, A.: Analysis of CCN activity of Arctic aerosol and Canadian biomass burning during summer 2008, Atmos. Chem. Phys., 13, 2735–2756, doi:10.5194/acp-13-2735-2013, 2013.

AMTD
7, 11137–11168, 2014

Marti, J. J., Weber, R. J., Saros, M. T., Vasiliou, J. G., and McMurry, P. H.: Modification of the TSI 3025 Condensation Particle Counter for pulse height analysis, Aerosol Sci. Tech., 25, 214–218, doi:10.1080/02786829608965392, 1996.

McDermott, W. T., Ockovic, R. C., and Stolzenburg, M. R.: Counting efficiency of an improved 30-Å condensation nucleus counter, Aerosol Sci. Tech., 14, 278–287, doi:10.1080/02786829108959490, 1991.

McMurry, P. H.: The history of condensation nucleus counters, Aerosol Sci. Tech., 33, 297–322, doi:10.1080/02786820050121512, 2000a.

McMurry, P. H.: A review of atmospheric aerosol measurements, Atmos. Environ., 34, 1959–1999, 2000b.

Mei, F., Hayes, P. L., Ortega, A., Taylor, J. W., Allan, J. D., Gilman, J., Kuster, W., de Gouw, J., Jimenez, J. L., and Wang, J.: Droplet activation properties of organic aerosols observed at an urban site during CalNex-LA, J. Geophys. Res.-Atmos., 118, 2903–2917, doi:10.1002/jgrd.50285, 2013.

Moore, R. H. and Nenes, A.: Scanning flow CCN analysis – a method for fast measurements of CCN spectra, Aerosol Sci. Tech., 43, 1192–1207, doi:10.1080/02786820903289780, 2009.

Moore, R. H., Nenes, A., and Medina, J.: Scanning mobility CCN analysis – a method for fast measurements of size-resolved CCN distributions and activation kinetics, Aerosol Sci. Tech., 44, 861–871, doi:10.1080/02786826.2010.498715, 2010.

Mordas, G., Manninen, H. E., Petäjä, T., Aalto, P. P., Hämeri, K., and Kulmala, M.: On operation of the ultra-fine water-based CPC TSI 3786 and comparison with other TSI models (TSI 3776, TSI 3772, TSI 3025, TSI 3010, TSI 3007), Aerosol Sci. Tech., 42, 152–158, doi:10.1080/02786820701846252, 2008.

O'Dowd, C. D., Aalto, P. P., Yoon, Y. J., and Hämeri, K.: The use of the pulse height analyser ultrafine condensation particle counter (PHA-UCPC) technique applied to sizing of nucleation mode particles of differing chemical composition, J. Aerosol Sci., 35, 205–216, doi:10.1016/j.jaerosci.2003.08.003, 2004.

Petters, M. D., Carrico, C. M., Kreidenweis, S. M., Prenni, A. J., DeMott, P. J., Collett Jr., J. L., and Moosmüller, H.: Cloud condensation nucleation activity of biomass burning aerosol, J. Geophys. Res., 114, D22205, doi:10.1029/2009jd012353, 2009.

Pöschl, U., Martin, S. T., Sinha, B., Chen, Q., Gunthe, S. S., Huffman, J. A., Borrmann, S., Farmer, D. K., Garland, R. M., Helas, G., Jimenez, J. L., King, S. M., Manzi, A., Mikhailov, E., Pauliquevis, T., Petters, M. D., Prenni, A. J., Roldin, P., Rose, D., Schneider, J., Su, H.,

AMTD
7, 11137–11168, 2014

Zorn, S. R., Artaxo, P., and Andreae, M. O.: Rainforest aerosols as biogenic nuclei of clouds and precipitation in the Amazon, Science, 329, 1513–1516, doi:10.1126/science.1191056, 2010.

Pruppacher, H. R. and Klett, J. D.: Microphysics of Clouds and Precipitation, Kluwer Academic Publishers Dordrecht, 1997.

Riipinen, I., Manninen, H. E., Yli-Juuti, T., Boy, M., Sipilä, M., Ehn, M., Junninen, H., Petäjä, T., and Kulmala, M.: Applying the Condensation Particle Counter Battery (CPCB) to study the water-affinity of freshly-formed 2–9 nm particles in boreal forest, Atmos. Chem. Phys., 9, 3317–3330, doi:10.5194/acp-9-3317-2009, 2009.

Rose, D., Gunthe, S. S., Mikhailov, E., Frank, G. P., Dusek, U., Andreae, M. O., and Pöschl, U.: Calibration and measurement uncertainties of a continuous-flow cloud condensation nuclei counter (DMT-CCNC): CCN activation of ammonium sulfate and sodium chloride aerosol particles in theory and experiment, Atmos. Chem. Phys., 8, 1153–1179, doi:10.5194/acp-8-1153-2008, 2008.

Rose, D., Nowak, A., Achtert, P., Wiedensohler, A., Hu, M., Shao, M., Zhang, Y., Andreae, M. O., and Pöschl, U.: Cloud condensation nuclei in polluted air and biomass burning smoke near the mega-city Guangzhou, China – Part 1: Size-resolved measurements and implications for the modeling of aerosol particle hygroscopicity and CCN activity, Atmos. Chem. Phys., 10, 3365–3383, doi:10.5194/acp-10-3365-2010, 2010.

Rose, D., Gunthe, S. S., Su, H., Garland, R. M., Yang, H., Berghof, M., Cheng, Y. F., Wehner, B., Achtert, P., Nowak, A., Wiedensohler, A., Takegawa, N., Kondo, Y., Hu, M., Zhang, Y., Andreae, M. O., and Pöschl, U.: Cloud condensation nuclei in polluted air and biomass burning smoke near the mega-city Guangzhou, China – Part 2: Size-resolved aerosol chemical composition, diurnal cycles, and externally mixed weakly CCN-active soot particles, Atmos. Chem. Phys., 11, 2817–2836, doi:10.5194/acp-11-2817-2011, 2011.

Rose, D., Gunthe, S. S., Jurányi, Z., Gysel, M., Frank, G. P., Schneider, J., Curtius, J., and Pöschl, U.: Size-resolved and integral measurements of cloud condensation nuclei (CCN) at the high-alpine site Jungfraujoch, Atmos. Chem. Phys. Discuss., 13, 32575–32624, doi:10.5194/acpd-13-32575-2013, 2013.

Saros, M. T., Weber, R. J., Marti, J. J., and McMurry, P. H.: Ultrafine aerosol measurement using a condensation nucleus counter with pulse height analysis, Aerosol Sci. Tech., 25, 200–213, doi:10.1080/02786829608965391, 1996.

AMTD
7, 11137–11168, 2014

Smith, J. N., Moore, K. F., McMurry, P. H., and Eisele, F. L.: Atmospheric measurements of sub-20 nm diameter particle chemical composition by thermal desorption chemical ionization mass spectrometry, Aerosol Sci. Tech., 38, 100–110, doi:10.1080/02786820490249036, 2004.

Snider, J. R., Wex, H., Rose, D., Kristensson, A., Stratmann, F., Hennig, T., Henning, S., Kiselev, A., Bilde, M., Burkhart, M., Dusek, U., Frank, G. P., Kiendler-Scharr, A., Mentel, T. F., Petters, M. D., and Pöschl, U.: Intercomparison of cloud condensation nuclei and hygroscopic fraction measurements: coated soot particles investigated during the LACIS Experiment in November (LExNo), J. Geophys. Res.-Atmos., 115, D11205, doi:10.1029/2009JD012618, 2010.

Sorjamaa, R. and Laaksonen, A.: The effect of H_2O adsorption on cloud drop activation of insoluble particles: a theoretical framework, Atmos. Chem. Phys., 7, 6175–6180, doi:10.5194/acp-7-6175-2007, 2007.

Stolzenburg, M. R.: An Ultrafine Aerosol Size DistributionMeasuring System, Ph. D. thesis, Mechanical Engineering Department, University of Minnesota, Minneapolis, 1988.

Stolzenburg, M. R. and McMurry, P. H.: An ultrafine aerosol condensation nucleus counter, Aerosol Sci. Tech., 14, 48–65, doi:10.1080/02786829108959470, 1991.

Stolzenburg, M. R. and McMurry, P. H.: Equations governing single and tandem DMA configurations and a new lognormal approximation to the transfer function, Aerosol Sci. Tech., 42, 421–432, doi:10.1080/02786820802157823, 2008.

Su, H., Rose, D., Cheng, Y. F., Gunthe, S. S., Massling, A., Stock, M., Wiedensohler, A., Andreae, M. O., and Pöschl, U.: Hygroscopicity distribution concept for measurement data analysis and modeling of aerosol particle mixing state with regard to hygroscopic growth and CCN activation, Atmos. Chem. Phys., 10, 7489–7503, doi:10.5194/acp-10-7489-2010, 2010.

Swietlicki, E., Hansson, H. C., Hämeri, K., Svenningsson, B., Massling, A., McFiggans, G., McMurry, P. H., Petäjä, T., Tunved, P., Gysel, M., Topping, D., Weingartner, E., Baltensperger, U., Rissler, J., Wiedensohler, A., and Kulmala, M.: Hygroscopic properties of submicrometer atmospheric aerosol particles measured with H-TDMA instruments in various environments – a review, Tellus B, 60, 432–469, doi:10.1111/j.1600-0889.2008.00350.x, 2008.

Wang, S. and Johnston, M. V.: Airborne nanoparticle characterization with a digital ion trap–reflectron time of flight mass spectrometer, Int. J. Mass Spectrom., 258, 50–57, doi:10.1016/j.ijms.2006.07.001, 2006.

AMTD
7, 11137–11168, 2014

Wang, X., Caldow, R., Sem, G. J., Hama, N., and Sakurai, H.: Evaluation of a condensation particle counter for vehicle emission measurement: experimental procedure and effects of calibration aerosol material, J. Aerosol Sci., 41, 306–318, doi:10.1016/j.jaerosci.2010.01.001, 2010.

Weber, R. J., Stolzenburg, M. R., Pandis, S. N., and McMurry, P. H.: Inversion of ultrafine condensation nucleus counter pulse height distributions to obtain nanoparticle (~ 3–10 nm) size distributions, J. Aerosol Sci., 29, 601–615, doi:10.1016/S0021-8502(97)10026-X, 1998.

Wiedensohler, A., Aalto, P., Covert, D., Heintzenberg, J., and McMurry, P. H.: Intercomparison of four methods to determine size distributions of low-concentration (~ 100 cm^{-3}), ultrafine aerosols ($3 < D_p < 10$ nm) with illustrative data from the Arctic, Aerosol Sci. Tech., 21, 95–109, doi:10.1080/02786829408959700, 1994.

Wiedensohler, A., Cheng, Y. F., Nowak, A., Wehner, B., Achtert, P., Berghof, M., Birmili, W., Wu, Z. J., Hu, M., Zhu, T., Takegawa, N., Kita, K., Kondo, Y., Lou, S. R., Hofzumahaus, A., Holland, F., Wahner, A., Gunthe, S. S., Rose, D., Su, H., and Pöschl, U.: Rapid aerosol particle growth and increase of cloud condensation nucleus activity by secondary aerosol formation and condensation: a case study for regional air pollution in northeastern China, J. Geophys. Res., 114, D00G08, doi:10.1029/2008JD010884, 2009.

Wimmer, D., Lehtipalo, K., Franchin, A., Kangasluoma, J., Kreissl, F., Kürten, A., Kupc, A., Metzger, A., Mikkilä, J., Petäjä, T., Riccobono, F., Vanhanen, J., Kulmala, M., and Curtius, J.: Performance of diethylene glycol-based particle counters in the sub-3 nm size range, Atmos. Meas. Tech., 6, 1793–1804, doi:10.5194/amt-6-1793-2013, 2013.

Wu, Z. J., Poulain, L., Henning, S., Dieckmann, K., Birmili, W., Merkel, M., van Pinxteren, D., Spindler, G., Müller, K., Stratmann, F., Herrmann, H., and Wiedensohler, A.: Relating particle hygroscopicity and CCN activity to chemical composition during the HCCT-2010 field campaign, Atmos. Chem. Phys., 13, 7983–7996, doi:10.5194/acp-13-7983-2013, 2013.

Zhang, R., Khalizov, A., Wang, L., Hu, M., and Xu, W.: Nucleation and growth of nanoparticles in the atmosphere, Chem. Rev., 112, 1957–2011, doi:10.1021/cr2001756, 2012.

Zhao, J., Eisele, F. L., Titcombe, M., Kuang, C., and McMurry, P. H.: Chemical ionization mass spectrometric measurements of atmospheric neutral clusters using the cluster-CIMS, J. Geophys. Res.-Atmos., 115, D08205, doi:10.1029/2009jd012606, 2010.

AMTD
7, 11137–11168, 2014

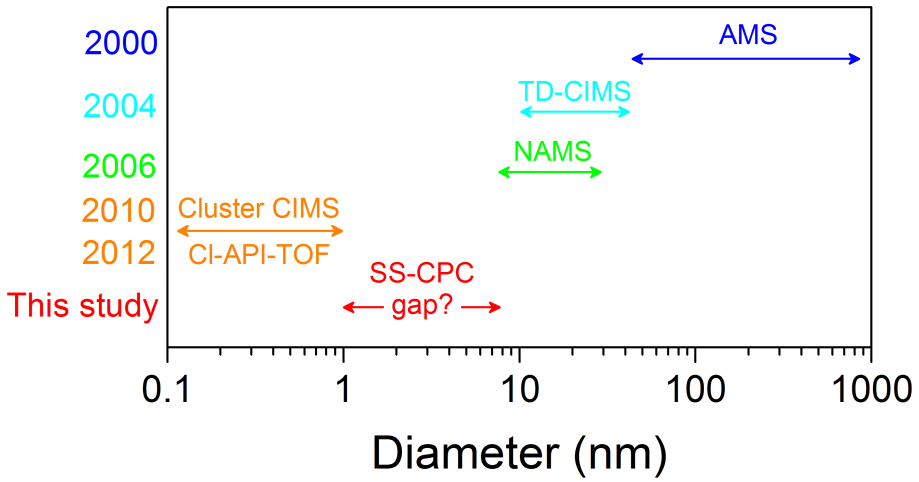

Figure 1. Size ranges of different measurement instruments in atmospheric aerosol research. The year when each technique was first reported is indicated on the left-hand side. Aerosol mass spectrometer (AMS) can measure particles with diameters down to ~ 40 nm (Jayne et al., 2000 and updated references on http://cires.colorado.edu/jimenez/ams-papers.html). Thermal desorption chemical ionization mass spectrometer (TDCIMS; Smith et al., 2004) and nano aerosol mass spectrometer (NAMS; Wang and Johnston, 2006) are commonly used at 10–30 nm particles. Analysis of molecular clusters with diameter up to ~ 1 nm has been achieved by cluster chemical ionization mass spectrometry (Cluster-CIMS; Zhao et al., 2010; Jiang et al., 2011a) and chemical ionization with the atmospheric pressure interface time-of-flight mass spectrometer (CI-APi-TOF; Jokinen et al., 2012). The use of scanning supersaturation CPC as nano-CCNC introduced in this study shall help to close the gap of 1–10 nm.

AMTD
7, 11137–11168, 2014

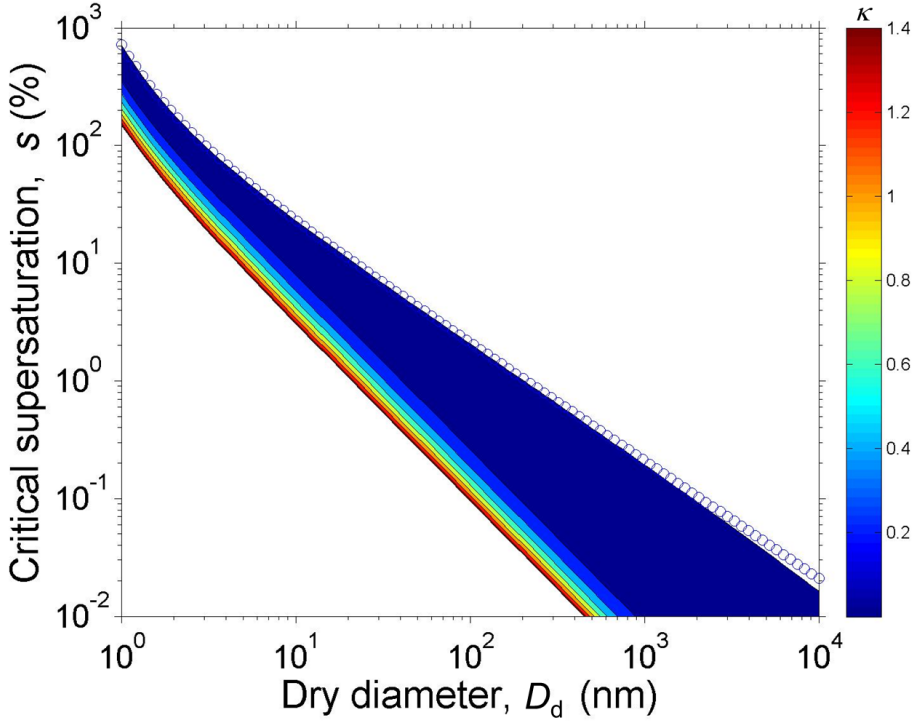

Figure 2. Critical water vapor supersaturation for the activation of particles with different dry diameter and chemical composition. The color bar indicates the κ values. The open circles are reference of water droplet.

AMTD
7, 11137–11168, 2014

Nano-CCN counter for size-resolved analysis of sub-10 nm particles

Z. B. Wang et al.

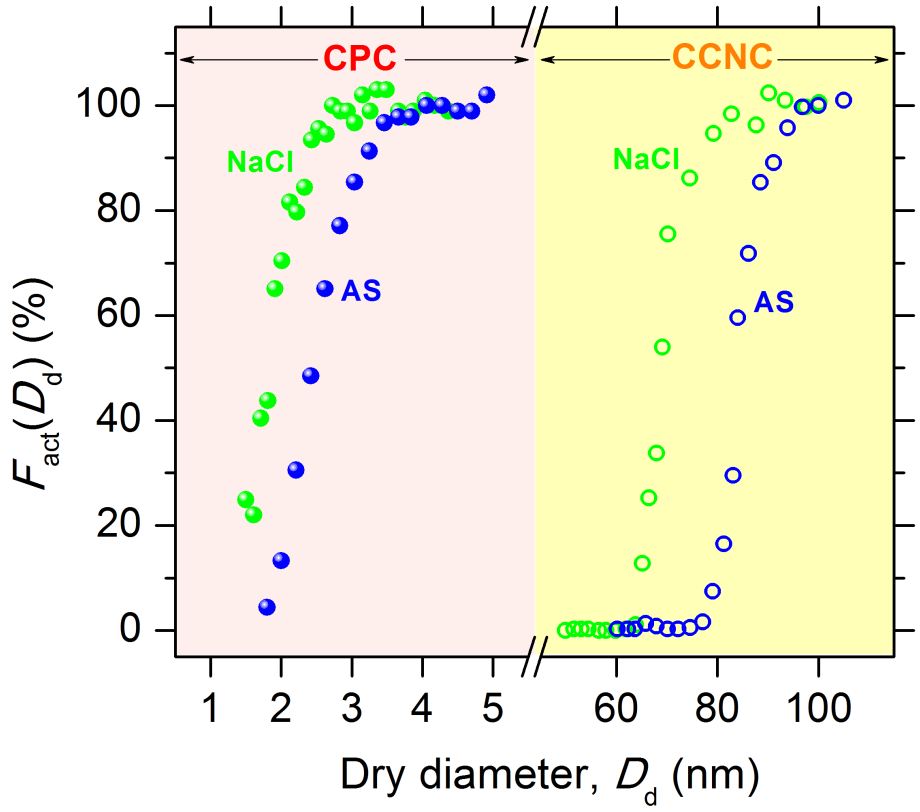

Figure 3. The symmetry between counting efficiency of a CPC (condensation particle counter, TSI model 3786) and the activation curve of a CCNC (cloud condensation nuclei counter, DMT CCNC). The green and blue circles represent the results for sodium chloride (NaCl) and ammonium sulfate (AS) particles, respectively. The CPC was operated with a growth tube temperature and a saturator temperature of 78 and 8 °C, respectively (Mordas et al., 2008). The CCNC was operated with a temperature difference of 4.5 K across the growth chamber (Moore et al., 2010).

AMTD
7, 11137–11168, 2014

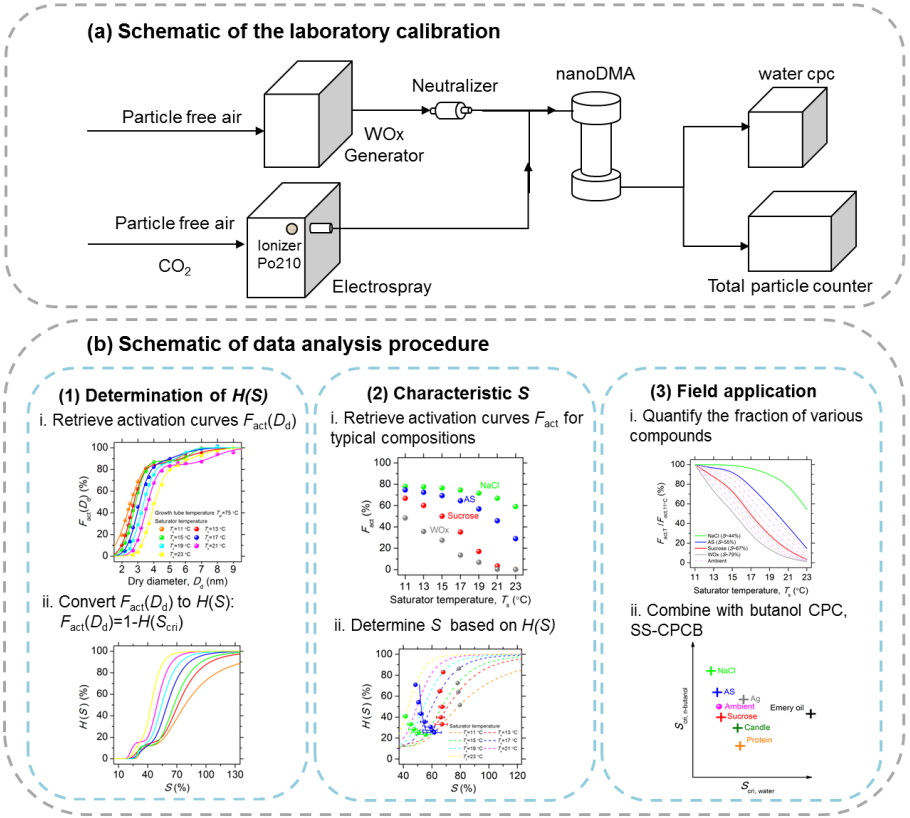

Figure 4. Schematics of the **(a)** laboratory calibration and **(b)** data analysis procedure for a SS-CPC used as nano-CCNC (Sect. 2.3 in the text).

AMTD
7, 11137–11168, 2014

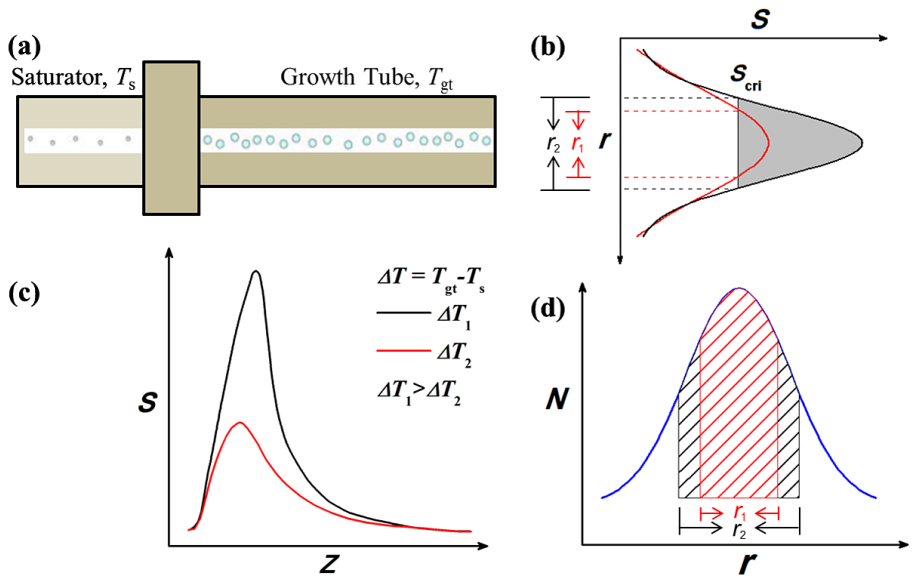

Figure 5. (a) Structure of the water CPC 3788 from TSI; schematic supersaturation S profiles **(b)** in the radial and **(c)** streamwise (according to Kulmala et al., 2007); the red and black lines indicate two different temperature differences between growth tube (T_{gt}) and saturator (T_s); the gray shadow represents the area where S is larger than the S_{cri} (critical supersaturation); r is the distance from the centerline and Z is the distance from the starting point of the growth tube. **(d)** Dimensions of activated particles (areas with lines); blue line is the schematic particle number distribution in the growth tube. The activated areas are determined by the distance along the radials shown in Fig. 5b.

AMTD
7, 11137–11168, 2014

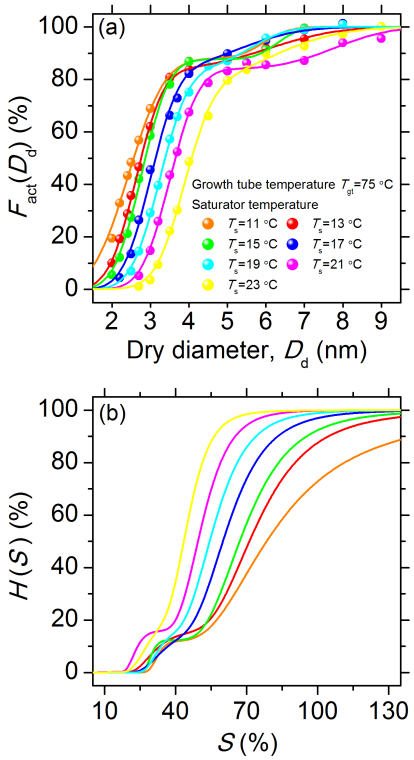

Figure 6. (a) Detection efficiencies of the SS-CPC (filled symbols) for WO_x particles. The water-based CPC 3788 was operated with a constant temperature of growth tube (T_{gt}) and the varied temperatures of the saturator (T_s). The different colored lines are fits of a bimodal lognomal cumulative Gaussian distribution function (Eq. 8) to the experimental points, corresponding to the different saturator temperatures. **(b)** Cumulative supersaturation distribution $H(S)$ inside CPC retrieved from the activation curve $F_{act}(D_d)$ based on Eq. (2). The colored solid lines indicate the different saturator temperatures, which are in line with **(a)**.

AMTD
7, 11137–11168, 2014

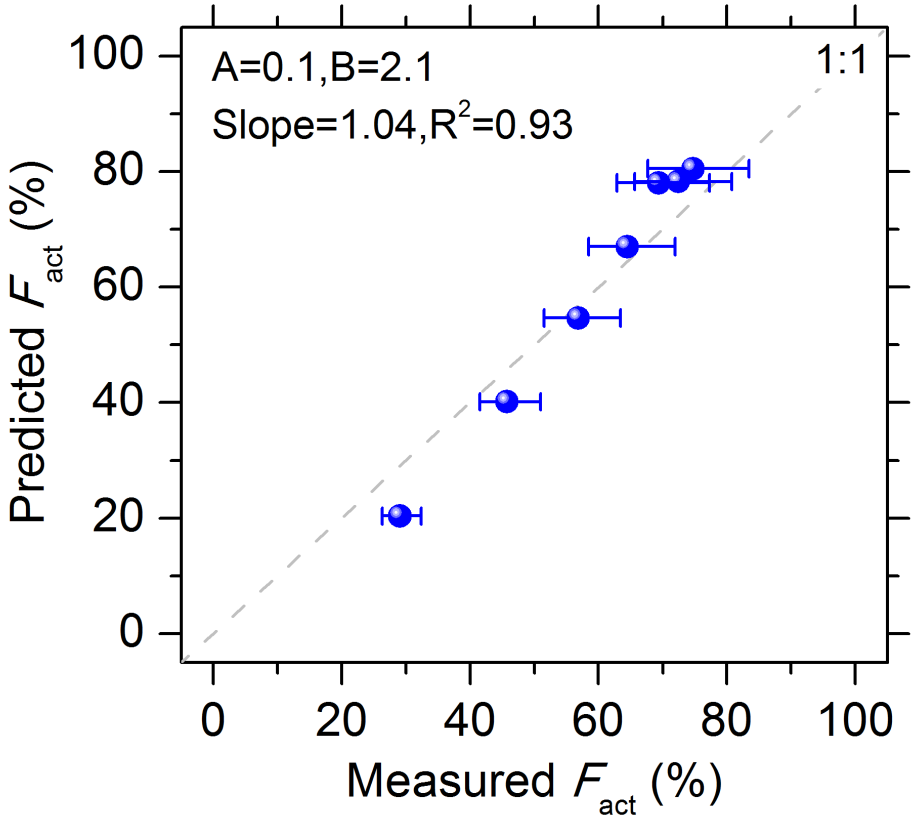

Figure 7. Comparison of measured activation fractions for 2.5 nm ammonium sulfate particles with those predicted from the revised Köhler equation including the FHH adsorption isotherm (Eq. 9 in the text). The whisker represents the standard deviation caused by the electrometer counting.

AMTD
7, 11137–11168, 2014

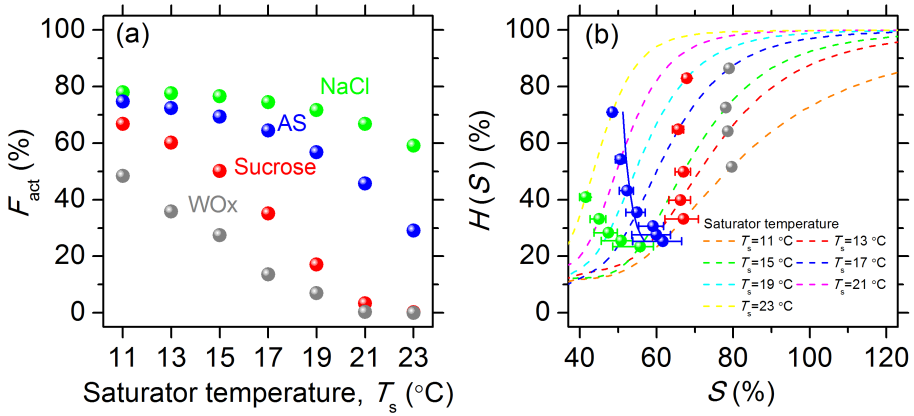

Figure 8. (a) Activation fractions for 2.5 nm NaCl (green), AS (blue), sucrose (red) and WO_x (gray) aerosols as a function of saturator temperature T_s. **(b)** Calculated critical supersaturations (filled symbols) for various chemical compounds based on the determined $H(S)$ (Fig. 6b) and measured F_{act} (Fig. 8a). The colored dash lines indicate the cumulative supersaturation distributions inside the nano-CCNC at different saturator temperatures. Solid line represents the theoretical critical supersaturation for 2.5 nm AS particles. The whisker represents the standard deviation caused by the electrometer counting. Note the points with uncertainties of S higher than 10 % are excluded.

AMTD
7, 11137–11168, 2014

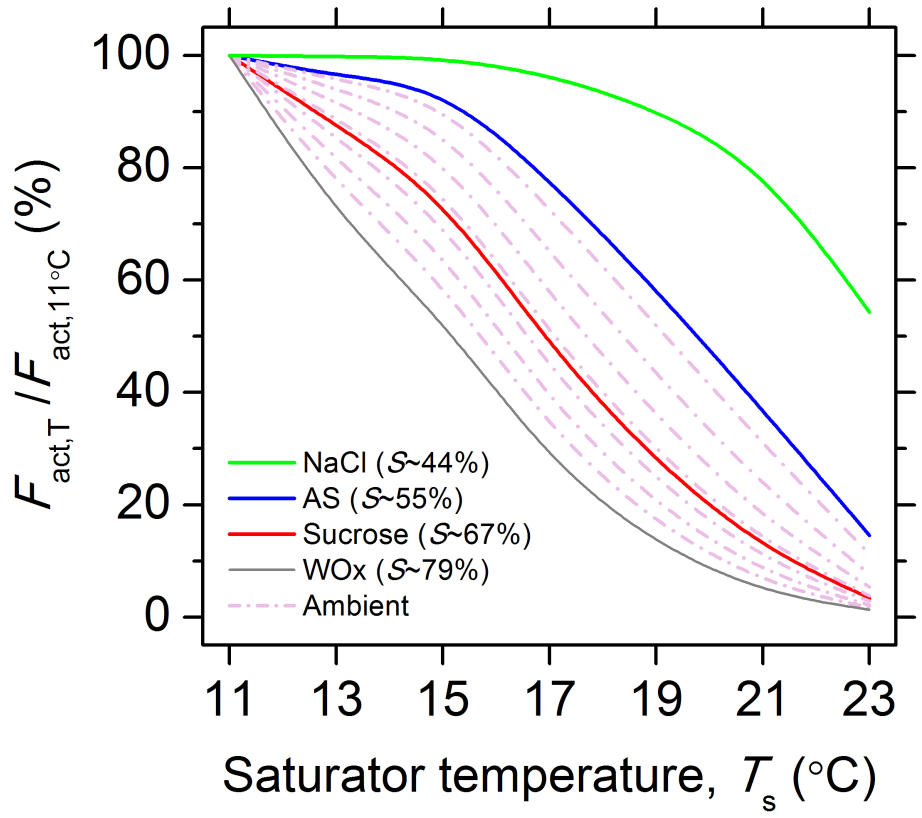

Figure 9. Profiles of relative activation ratio as a function of saturator temperature. The critical supersaturations for NaCl, AS, sucrose and WO_x are average values at seven saturator temperatures. The dash dot lines represent the compounds with critical supersaturation in the range of 57 to 75 %, during which is indicative of ambient nanoparticles.

AMTD
7, 11137–11168, 2014

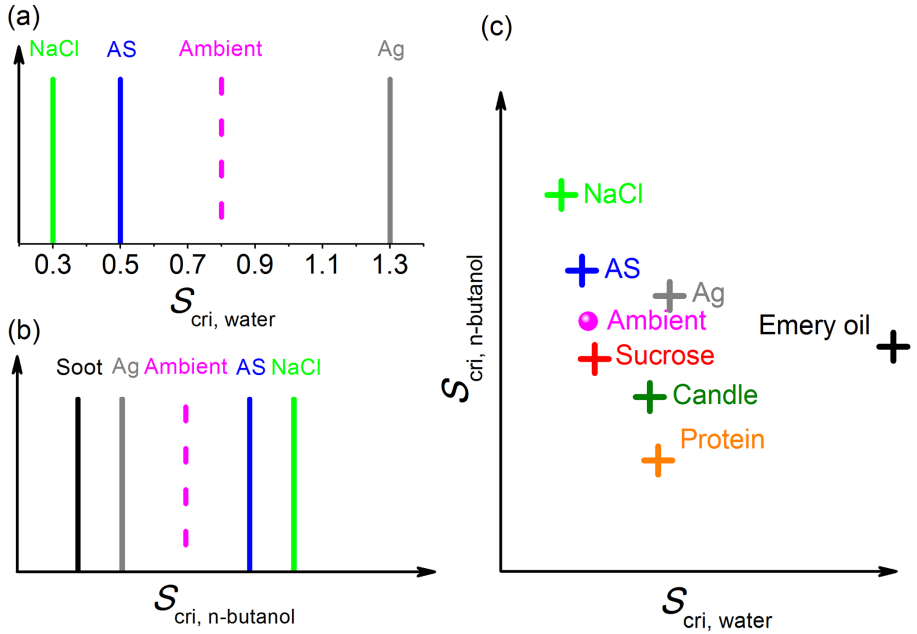

Figure 10. Critical supersaturations (S_{cri}) for various chemical compounds in different working fluids: **(a)** water and **(b)** *n* butanol. **(c)** Schematic of 2-D solvoscopicity distribution matrix. The data set is collected from the previous studies (Hermann et al., 2007; Kulmala et al., 2007; Wang et al., 2010; Kupc et al., 2013).

AMTD
7, 11137–11168, 2014

Nano-CCN counter for size-resolved analysis of sub-10 nm particles

Z. B. Wang et al.